Neo Science Peer Reviewed Journal
Volume 5, Jan. 2023 ISSN (E): 2949-7701
www.neojournals.com

FEATURES OF STRUCTURAL STRUCTURE AND RELATIONSHIPS OF BASALT FIBRES FOR APPLICATIONS

Oybek Oripov1*, Jamoliddin Kuljonov1, Gavhar Narmayeva1,
Muqaddas Abdushukurova2
1Samarkand State University, Samarkand 140104, Uzbekistan
2National University of Uzbekistan named after Mirzo Ulugbek, Tashkent 100174, Uzbekistan
Author: oripovoybek0103@gmail.com (O. Oripov)

Abstract:

Continuous basalt fibres offer a unique combination of good mechanical and functional properties at an affordable price level. These properties can be useful in high-performance polymer matrix composites, where cost orientation and function integration become priority goals. In this work, a currently unsolved problem of basalt fibres related to high productivity is considered: the variation of the structural and mechanical properties of the fibre due to the inhomogeneity of the natural raw materials and the spinning process. Commercial basalt fibres from seven different manufacturers were studied for their fibre chemistry, diameter distribution, and occurrence of defects and crystallites. In the second stage, structure-property relationships of different scales were established with one fibre.

Keywords:

Mechanical properties of basalt fibers; polymer matrix; aluminum oxide; aerospace grade; vacuum; composites.

1. Introduction

In recent years, continuous basalt fibres (CBF) have attracted more and more interest in the scientific and industrial composites community [1,2]. Modulus and strength values for high-grade basalt fibres are between E- and S2-glass fibres. With a higher performance-to-cost ratio compared to common glass fibres, basalt fibres address the increasing cost trend across industries currently using FRP. The thermal, chemical and tribological resistance and thermal insulation properties of basalt fibres can be an added value in integrated composite structures. For applications of basalt fibres in high-performance fields such as aeronautics, the expected spread in the structural and mechanical properties of CBF is very important. Variations can be caused by the natural raw materials used and complications in the basalt fibre spinning process [3]. This aspect requires further investigation before using CBF in high-performance applications. Reproducible, measurable and permanent material properties are a prerequisite for lightweight and safe design. Choosing the appropriate basalt rock as raw material determines the composition of chemical fibres similar to synthetic glass fibres in basic oxides. The melt spinning process currently used to produce CBF requires more than 46% silicon (SiO_2) [4]. Higher percentages further improve the spinning process [5] and improve the mechanical properties of the fibres. Similarly, alumina (Al_2O_3) improves mechanics depending on its quantity [6]. The main difference between basalt and fibreglass is the high percentage of iron. The amount and percentage of iron (Fe_2O_3) and iron (FeO) affect the thermal and crystallization properties of iron, as well as the mechanical and optical properties of CBF

[7–11]. Additional oxides commonly present in CBF are CaO, MgO, Na, K_2O and TiO_2. The stages of the CBF spinning process have been described by several authors in the literature [3,12]. At a given solution chemistry, pressure and draw speed, high-quality filaments can only be spun within a specific temperature process window. A mismatch can lead to solution leakage, fibre breakage, defects and deterioration of mechanical properties. Basalt fibres have a narrower processing window than glass and a higher variation of processing conditions along the nozzles of the bush. In Figure 1, the temperature process window (horizontal boundaries) and process parameter variation (vertical error bars) are schematically compared between E-glass and basalt fibres. The processing window of stable fibre formation from vitreous solutions is mainly determined by the ratio of viscosity and surface tension [11,12]. The high content of silicon, alumina and iron in basaltic rock causes high viscosity and high rotation temperature [6,10,13]. In addition, the strong temperature dependence of viscosity narrows the temperature window [14]. Additional retention at high temperatures is caused by the high hydration of basalt melts in the platinum-rhodium handle [15]. Due to the reduced contact angle, the solution can spread over the surface of the bush instead of forming a stable rotating cone. As an additional effect, glass fibres were labelled with EGF, RGF, and S2GF, respectively.

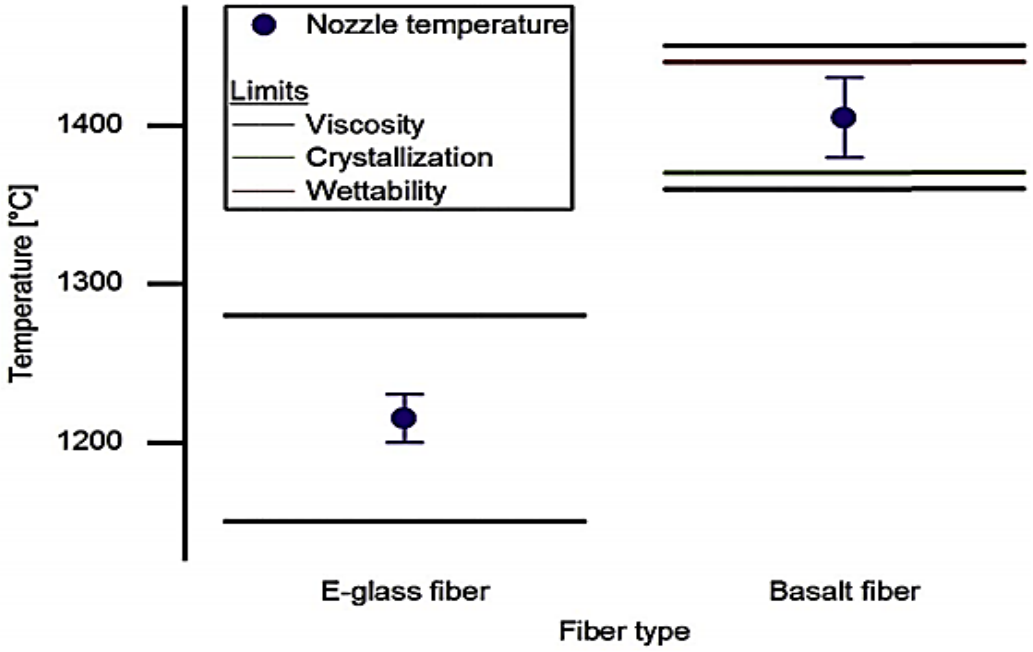

Figure 1. Spinning limits and uniformity of basalt and E-glass fibre. Values for temperature windows are adopted by Ivanitsky [14].

2. Experimental

2.1. Materials

Continuous basalt fibres from seven manufacturers were studied. Fibre samples were obtained as roving with the target specifications: fineness of 600 tex, an average diameter of 9 μm, and a size compatible with silicone-based epoxy. Basalt roving samples are labelled CBF1 to CBF7 to distinguish the seven manufacturers. Roving from three manufacturers (CBF1, CBF4 and CBF5) was obtained from three different production dates more than one week apart. These different spinning batches are indicated by an

additional number (eg CBF4.2). Aerospace grade E-, R-, and S2- glass fibres designated EGF, RGF, and S2GF, respectively, were included as reference fibres. 6 epoxy resin was used to produce composite laminates and embedded roving specimens.

2.2. Analysis and test methods

2.2.1. Chemical composition

The composition of chemical fibres in mass and mole fractions of oxides was calculated from the results of sequential energy dispersive X-ray spectroscopy (EDX) and Moessbauer spectroscopy. Chemical composition data were evaluated for variability (e.g., between batches of materials) by calculating pooled standard deviations according to equation (1) [16]. First, the standard deviation is calculated in atomic percent for each of the nine components compared compositions. In order to determine the fibre diameter distribution, the spinning parts are impregnated with high-resin-fibre contrast resin. After mounting, the samples were cut in a plane perpendicular to the direction of the fibres, ground and polished. The profile of the entire roving was recorded with a Carl Zeiss AX 10 optical microscope using a resolution of nine pixels per 2 μm. ImageJ's contrast threshold function was applied to the image to distinguish fibre and matrix areas. The equivalent diameter for each fibre can be calculated from the corresponding pixel areas. The lengthwise deviation of fibre diameters was determined by scanning electron microscopy (SEM). 200 mm filament sections were measured in 20 mm diameter increments.

2.2.3. Crystalline

X-ray diffraction (XRD) was performed on a Seifert XRD 3003 TT powder diffractometer using CuK.radiation with al = 1.54 Å. The fibres are ground with lime and mortar. The collection of XRD patterns took place in the scanning phase of 2θ = 0.05° and at a scanning speed of 3° 2θ/min in the angular range of 2θ = 10-70°.

2.2.4. The density of defects

Fibre defect density was checked based on single fibre strength data (see 2.2.6.). The scale parameters and the local Weibull modulus are graphically defined in the Weibull diagram of the two-parameter Weibull distribution [17]. Then, the average filament strength at each of the four measurement lengths is calculated. Basalt fibres are usually brittle and show the characteristics of failure of the weakest joints [18,19]. Testing at different gauge lengths changes the size and surface area of fibres that can be affected by defects. As a result, fibres with a high defect probability show a strong decrease in strength at high gauge lengths, while a perfect fibre maintains its strength value at low gauge lengths. To use this behaviour for defect density inferences, average power values are plotted against different gauge lengths. According to the weakest link theory, the data points form a straight line on a log-log plot assuming a unimodal defect distribution.20]. The average Weibull modulus was determined from the slope of the linear fit equal to r −1/r [.21,22]. A high value of r indicates a slight decrease in strength with a larger length and a lower defect density.

2.2.5. Fibre Density and Spinning Fineness Data on fibre density is required for all mechanical testing methods including vibroscopic diameter measurement and fibre volume calculation. The mass of about 3 g of twisted fibres is measured at 450°C until constant mass. Subsequent density measurements were performed on a Quantachrome

Ultrapycnometer 1000 with helium purge gas. In addition, embedded and composite tensile tests require fineness values defined as mass per unit length of the conductor. Using the gravimetric method, ten 5 m long rolling pieces were cut, sized to constant mass at 450 °C, and finally weighed with an accurate balance.

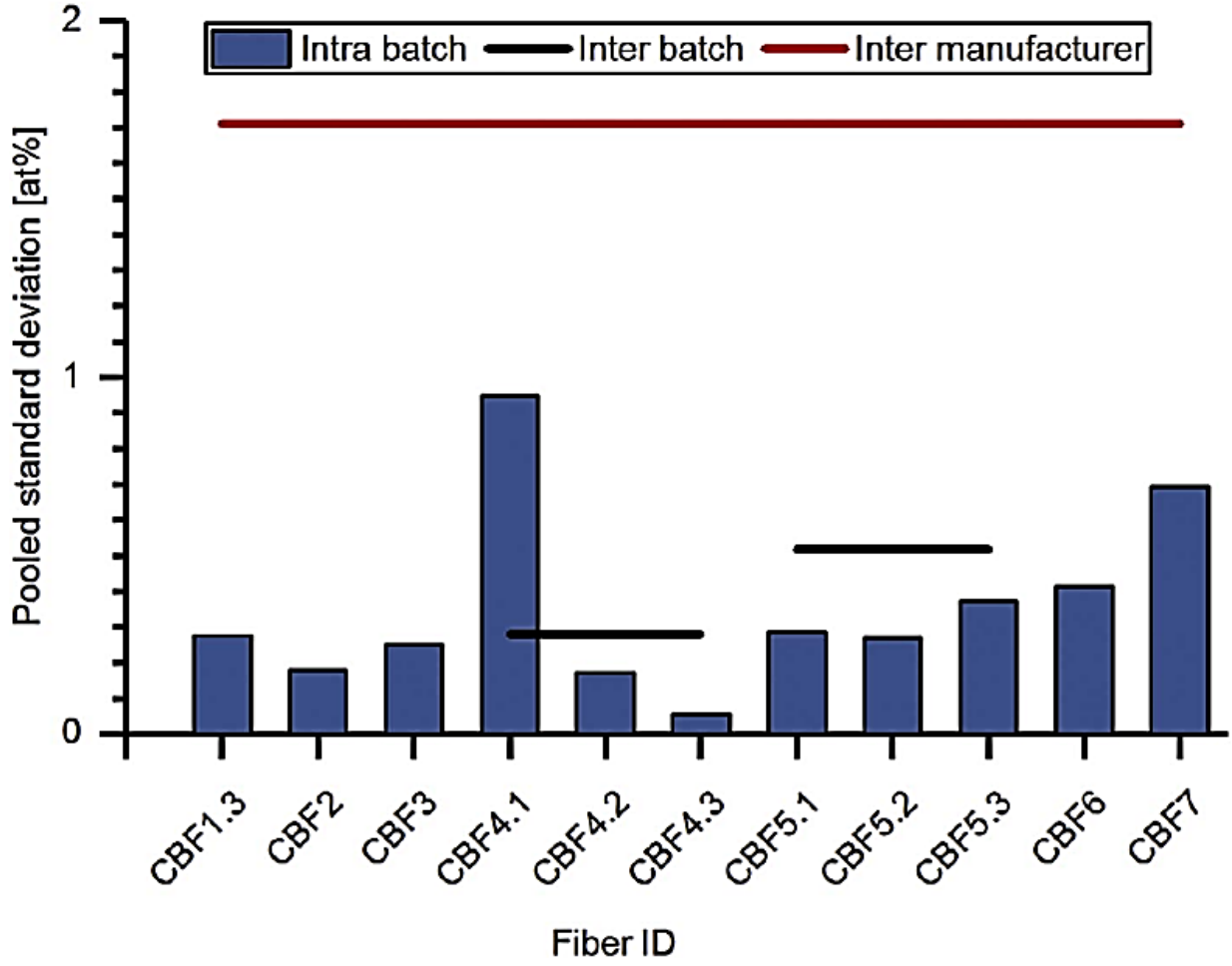

Figure 2. Basalt fibre of chemical compositions CBF1-CBF7 pooled standard deviation.

2.2.6. Single fibre tensile test

The mechanical properties of the single fibres were tested on a Favimat + single fibre tensile testing machine. The equipment is equipped with a vibroscopic unit to determine the fineness of the compressed filament by measuring the resonance frequency. With a known value for the fibre density, the diameter of the filament can be calculated from its fineness. The following gauge lengths and a number of samples (in parentheses) were measured: 10 mm (20), 20 mm (50), 50 mm (20), and 95 mm (20). The vibroscopic method gave the same diameter distributions as the optical method in Section 2.2.2. A strain rate of 10%/min was used at all measurement lengths. To minimize the effect of compressive stiffness, Young's modulus was determined at 0.25 and 0.50% strain at a maximum gauge length of 95 mm.

2.2.7. Impregnated roving tensile test

Rotating parts are vacuum-impregnated with epoxy resin (VAP)®). A proper load input and compression area were created by adhesively glueing dried GFRP tabs. Specimens

with a free compression length of 150 mm were subjected to a test speed of 5 mm/min in a Zwick Z250 testing machine. Displacement was recorded with a multi tens extensometer. Young's modulus was estimated in the strain range of 0.25–0.50%. Modulus and strength values are based on 100% fibre content (FVC) using the rule for the mixture normalized.

2.2.8. Composite tensile test

The mechanical properties of the composites were determined by unilateral fibre-reinforced samples of CBF1.3, CBF4.3, CBF5.1 and S2GF fibres impregnated with epoxy resin. Textile preforms were produced by aligned fibre placement (TFP) according to the procedure described by Gnädinger [23]. In this technique, the roving is oriented and attached to the carrier fabric by a zigzag stitch. In order to avoid the introduction of thread material into the sample, the thread and the carrier fabric are cut in the test area, and then fixation is continued in the residual areas. A nominal laminate thickness of 2 mm and a fibre volume of 55% were achieved by adjusting the number of layers and the spin coating. The infusion of the preform with epoxy resin took place in the VAP technique. After cutting, the ISO 527-5 type specimens were fitted with pre-glass load insertion and strain gauges. Testing was performed on a Zwick Z250 testing machine at a testing speed of 2 mm/min. A strain of 0.25 to 0.50% was used to estimate modulus, with both modulus and strength normalized to 55% FVC.

3. Results and discussion

3.1. Structural analysis

3.1.1. Content

Basalt rock is a natural material formed by the cooling of magma after the eruption. As a result of this undefined natural formation process, basalts from different geological locations may differ in chemical composition. In addition, additives and impurities can cause chemical homogeneity within the mine. By using basalt rock as a raw material for fibre spinning, these chemical changes can be transferred to the product and its properties. The chemical composition of basalt fibres can be determined by several methods, including EDX, X-ray fluorescence (XRF), X-ray photoelectron spectroscopy (XPS), and XRD. The methods vary in accuracy, cost, measured volume, and requirements for sample amorphousness or crystallinity. EDX was chosen in this study because it is a relatively fast, simple and popular method with sufficient accuracy to detect changes in industrial processes. Additionally, Moessbauer measurements were performed to differentiate the oxidation state of iron elements. Figure 2 shows the degree of variation in chemical composition found in different basalt fibres. Pooled standard deviations of elemental fibre content are calculated to assess variation within and between batches, as well as between fibre manufacturers. Several fibres were measured from each fibre batch. Intra-batch variations may be due to EDX measurement error and insufficient homogenization during the melting of basalt for fibre spinning. Several fibre batches from different production dates were measured for CBF4 and CBF5. Variation between batches may be due to inhomogeneity within the quarry, which is not compensated for in the material selection and cleaning process. According to Figure 2, the inter- and intra-batch variations are below 1%. In comparison, the deviations between manufacturers are greater. This indicates significant differences in chemical composition between producers' quarries as a result of different geological locations. Therefore, the choice and change of raw material quarry are considered key decisions. Because of the complex interactions of

the nine different oxides, as well as the relationship between chemistry and fibre processing window, it is difficult to predict fibre properties based on chemical composition data alone. Nevertheless, a higher glass-forming content was found to improve the mechanical performance of basalt fibres (see section 3.2.1.).

3.1.2. Diameter

The diameter of the filament represents another important parameter of the reinforcement component. Typical values for the average diameter of high-quality structured glass fibres are in the range of 9-10 μm. This value represents a compromise between three elements: good fibre strength due to size effect, high specific surface area for fibre-matrix bonding, and critical length-to-diameter ratio for respirability and potential carcinogenicity. preventing fibre fragments. According to the size effect, the strength of the fibre depends on its diameter. Smaller diameter specimens often have higher strength due to the reduction of possible flaw size in the reduced specimen size. The diameter of basalt and fibreglass is determined by the parameters of the solution-spinning process. Thus, nozzle diameter, draw speed, solution pressure and viscosity are the main influencing factors. In contrast, the fibre diameter distribution is a good indicator of the homogeneity of the spinning process. High dispersion of fibre diameters may result from unfavourable variations in processing parameters [24]. As mentioned above, the chemical composition can additionally affect the processing properties of the solution and therefore indirectly affect the resulting diameter. Figure 3 shows the distribution functions of diameters from optical microscope measurements of all fibre diameters along a piece of roving. The number of data points ranges from 1400 to 3600, corresponding to the number of filaments in the roving. Basalt fibre spinning is usually limited to 400 nozzles [12]. Checked rovings are assembled from several direct rovings. Basalt fibres CBF2, CBF6 and CBF7 show a relative distribution of fibre diameters in the range of 15.6–16.9%. CBF1, CBF3, CBF4, and CBF5 show an intermediate prevalence of 10.2–14.3%. A narrower distribution of the latter indicates a more homogeneous spinning process due to the manufacturer's process control. Measurement of different batches of material for CBF1, CBF4 and CBF5 revealed low batch-to-batch variation. None of the basalt fibres achieved the low diameter variation of 6.0% to 8.6% of the glass reference fibres EGF, RGF, and S2GF. The low diameter variation of glass fibres is mainly due to the high thermal uniformity during the spinning process. Unlike infrared-absorbing basalt solutions, the second dimension of diameter variation is along the length of the fibre. A reduction in fibre diameter acts as a crimp and may indicate a weak point under mechanical loading. Along with filament sections, SEM diameter measurements yielded variations of 1.0% to 1.5%. The change in fibre diameter along the length of the basalt fibres is of the same magnitude as the glass fibre. The measurement accuracy was determined to be 0.3% based on repeated diameter measurements at the same point.

3.1.3. Crystallization

Crystallites grown during fibre spinning can act as defects and reduce fibre strength. Manylov [8] showed that the first type of crystallite that usually appears during the thermal treatment of basalt fibres is spinel magnetite, which has strong peaks at 2θ angles of 36° and 64° in the XRD pattern. Later pyroxene, hematite and plagioclase. XRD plots in Fig. 4 do not show sharp peaks for CBF1-CBF7, indicating the presence of magnetite or other types of crystallites. An amorphous peak is visible in each pattern for CBF1-CBF7 and the glass fibre indicates S2GF and EGF. Wei [25-28] and Greek [19] analyzed

the pile condition by Scherrer's equation and made conclusions on the effect of fibre microstructure and mechanical performance. The basalt fibre nodules Fig. 4 are very similar and do not show major microstructural differences.

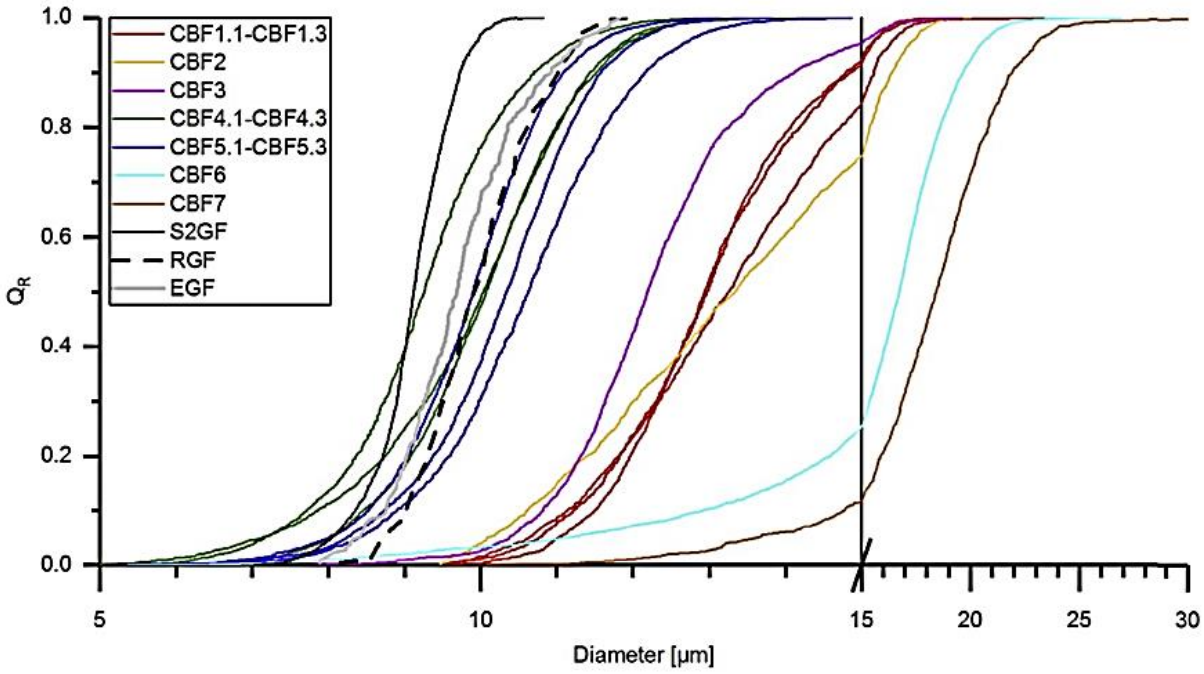

Figure 3. Diameter distribution in a cross-section of different glass and basalt fibre rovings.

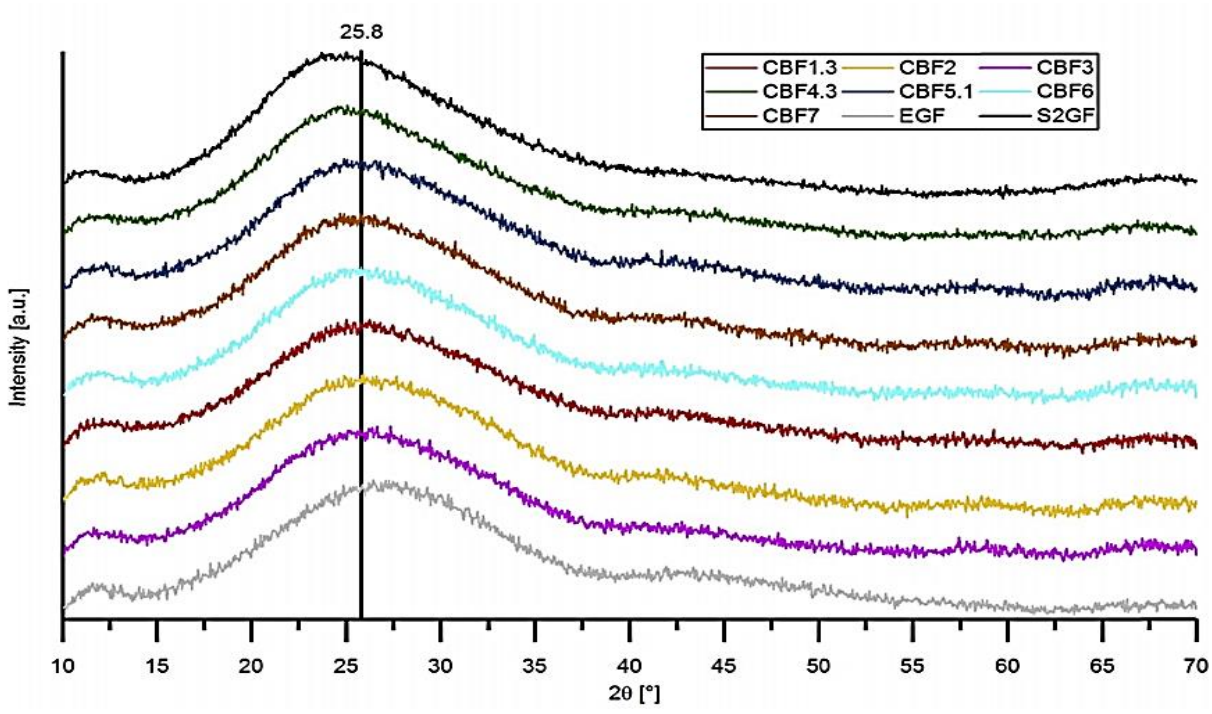

Figure 4. X-ray diffraction patterns of basalt and glass fibres. The average peak centre position for basalt fibres is 25.8° at an angle of 2θ.

3.1.4. Disadvantages

Although crystallites do not appear to be the main source of defects in the fibres under investigation, fibre defects may occur during spinning outside the processing window. 2.2. As described in 4., single fibre strength values at different gauge lengths can provide information on defect density. The line plots and values for the mean Weibull modulus r in Figure 5 provide a comparison of the steel and glass fibres in terms of defect density. S2GF aeronautical reference fibres have a high value for r, indicating a low defect density. Correspondingly, this is seen in the small dip of the black fitting line at higher wavelengths. In contrast, EGF shows many defects. This may be due to the low silica content of Eglass, which complicates the spinning process. CBF1, CBF4 and CBF5 already showed low diameter changes and also show low defects. density. In contrast, CBF2 has the highest defect density among all investigated basalt fibres.

3.2. Structure-property relations

The second part of the results is related to the effect of structural properties on the mechanical performance of fibres. The results of a single fibre, impregnated roving and unidirectional composite tensile tests serve as a basis for comparison. This methodology is based on the logic of reduced sensitivity to individual fibre properties. The composition of the chemical fibre can greatly affect the mechanical properties of the fibre [4]. Different roles are assigned to structural oxides: glass formers create an interconnected network of chemical bonds. Glass modifiers modify this network, while intermediates can take on both roles. The proportion of silica and magnesium, in a certain range, alumina can play the role of glass-forming oxides [6]. Fibre diameter is the second design parameter studied in this section. Larger fibre diameters can increase the probability of defect and failure due to the size effect. The effect of basalt fibre chemistry on mechanics, as well as the effect of diameter on mechanics, is specified separately in Section 3.2.1. and 3.2.2. The average diameter and amount of glass formers for each fibre in the preparative investigation were plotted on a xy diagram. Due to the correlation with the viscosity of the solution, the relationship between both parameters was suspected. It can be verified that there is no correlation between the data points determined by the composition and diameter of the glass formers.

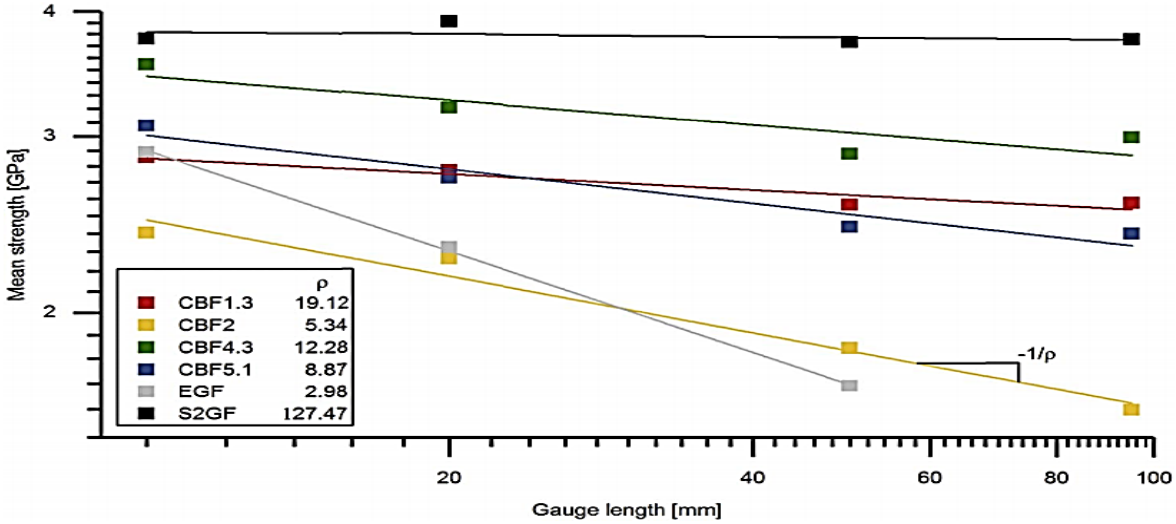

Figure 5. Average single fibre strength and obtained average Weibull modulus at different gauge lengths.

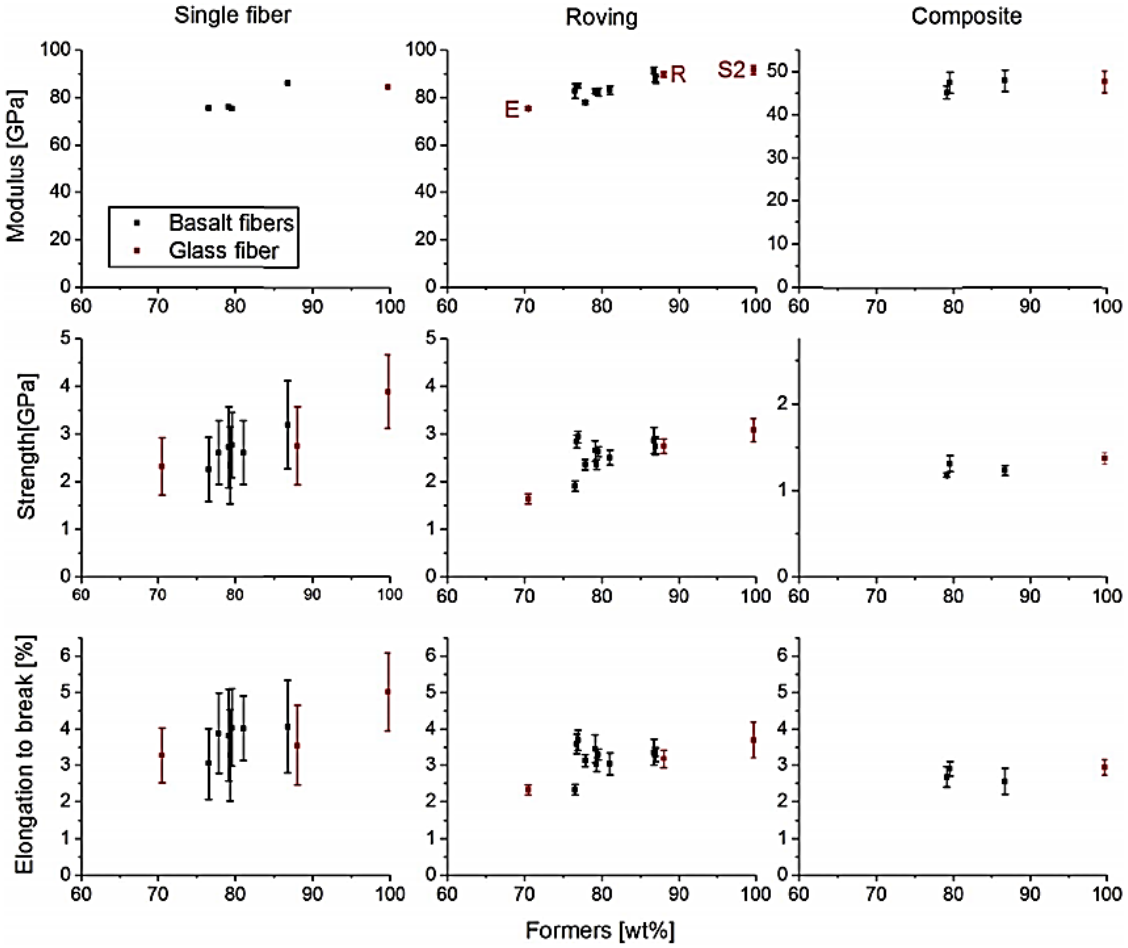

Figure 6. Mechanical properties are related to the proportion of glass-forming oxides. Single fibre strength and elongation at break were determined at 20 mm gauge length, and single fibre modulus at 95 mm gauge length.

3.2.1. Glass formers and mechanics

According to the single fibre and impregnated roving tensile test results in Figure 6, the mechanical properties of basalt and fibreglass are clearly affected by the number of glass formers. Modulus, strength and elongation at break increase with a higher percentage of oxide formation. Thus, a common trend is observed for glass and basalt fibres. Regarding the number of glass formers and the obtained mechanical properties, basalt fibres are between E- and S2-glass fibres. Due to the relationship between chemistry and mechanics, it is very important to monitor the chemical composition of basalt raw materials and fibre with appropriate test methods. The trend of improved mechanical performance at higher glass content can be useful for evaluating mechanical fibre performance. However, it is difficult to predict. Compared to other tensile test methods, Figure 6 shows a higher dispersion due to the weakest bond failure behaviour of single fibre strength results. The degree of strength of weak single fibres determines the magnitude of rotational force. At a certain point, the accumulation of the weakest filament failure, despite the existing transfer of loads between the fibres of the impregnated yarn, begins to break the cycle. Composite mechanical properties are less sensitive to the glass-forming content of the reinforcement. The strength and elongation at break are even lower in the composite. The low sensitivity and magnitude of the

composite mechanical index can be explained by the effects of the manufacturing process, such as fibre orientation, defects, voids, and porosity. In addition, for example, matrix 3 and interphase properties are gaining importance.

3.2.2. Diameter and mechanics

Figure 7 relates the mean diameter to the mechanical properties of basalt fibres to reveal the potential effect of size. To focus the comparison on size effect and diameter aspects, the additional effect of differences in fibre chemistry is reduced by considering only basalt fibres with similar glass content. Important Effects of Different Basalt Fibre Chemistry on Mechanics 3.2.1. will be considered separately in the section. The average values for tensile strength and elongation in the single fibre and impregnated roving test method tend toward higher values for lower average diameters. However, the trend is less clear than the effect of glass manufacturers, as it varies within the variation of the test. results. The inverse relationship between fibre failure and diameter can be explained by the high volume of the material and the possibility of defects in large-diameter filaments, which leads to a decrease in strength. In the composite results, the paucity of suitable data points with similar glass composition allows for poor interpretation. Because of the previously observed small sensitivity of the composite values to the number of glass formers, the diameter effect, which is less pronounced than the chemical effect, is also expected to dominate the matrix and interphase properties.

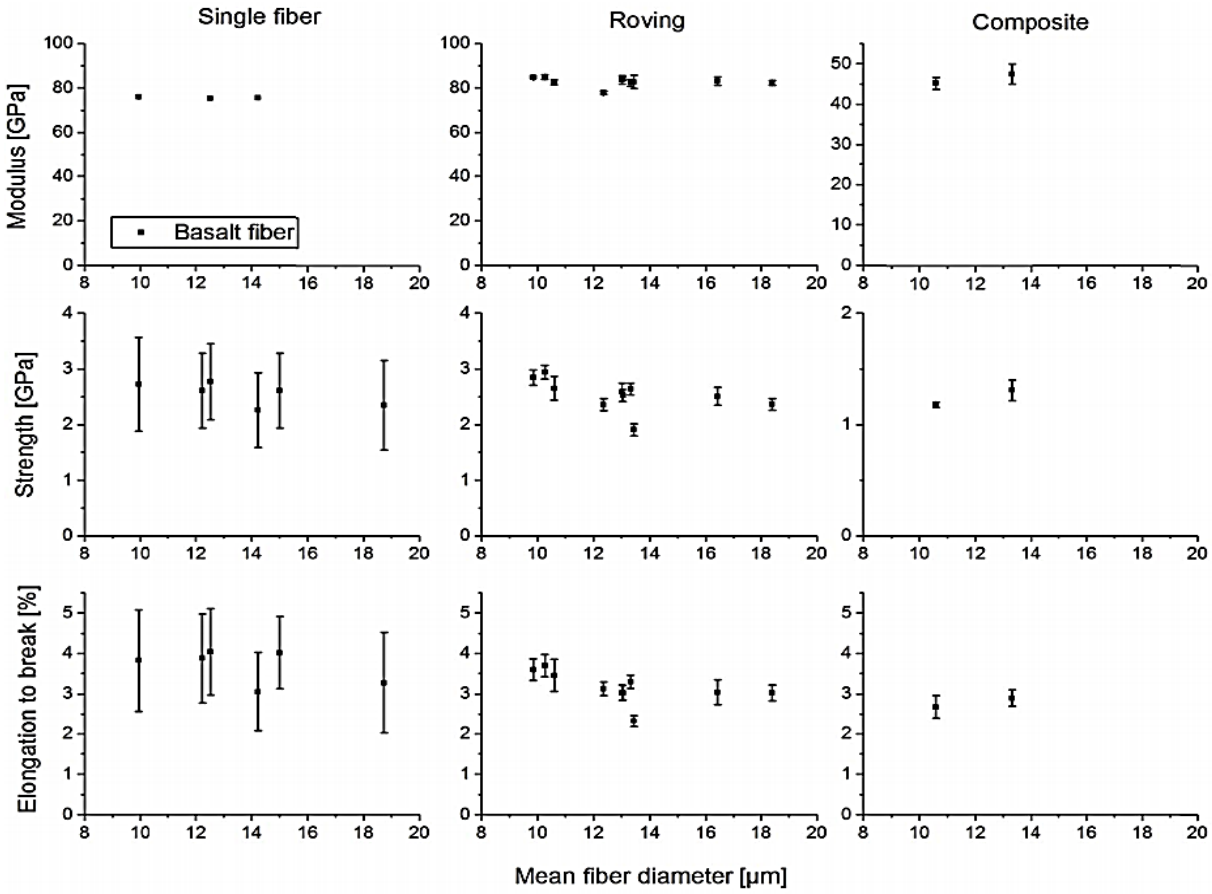

Figure 7. Effect of average fibre diameter on mechanical properties of basalt fibres with a similar composition of glass-forming oxides. Single fibre strength and elongation at break were determined at 20 mm gauge length and single fibre modulus at 95 mm gauge length.

4. Conclusions

The structure of continuous basalt fibres was analyzed for changes in raw material selection and the spinning process.

•Despite using natural basalt rock as raw material, the measured batch-to-batch variation in chemical fibre content is less than 1% of the total standard deviation.

•Percent variations in fibre diameter of basalt fibres showed a wide spread from 10.2% to 16.9%, indicating varying degrees of control of the spinning process among the seven manufacturers evaluated. A higher diameter variation (6.0%–8.6%) was found for basalt compared to the fibreglass reference. This can be explained by the increased thermal uniformity due to the transparency and thermal insulation of the basalt solutions during the spinning of basalt fibres.

•Despite the narrower temperature window for fibre spinning, continuous basalt filaments can be produced without a significant content of crystallites and with an acceptable number of defects. The mechanical properties of basalt fibre are between E- and S2-glass. The influence of the fibre structure and the resulting changes on the mechanical properties of the fibres are evaluated by formulating the structure-property relationships.

• For basalt fibres, an inverse trend of elongation and break strength are observed as the mean fibre diameters increase and is related to the size effect.

• Mechanical properties of basalt and glass fibres increase with higher amounts of silicon, alumina and magnesium (glass formers). The selection of raw materials and the spinning process of continuous basalt fibres determine the quality and properties of the fibre in a dimensional way. Basalt fibres with controlled chemistry, diameter and microstructure can be used in high-performance industries. Further work will examine the adhesion and interphase properties of basalt fibre, dimensions, and thermoset resins, and investigate whether the mechanical properties of basalt fibre can be transferred to composites.

References

[1]Fiore V, Scalici T, Di Bella G, Valenza A. Review on basalt fibre and its composites. Compos B Eng 2015;74: 74–94.

[2]Dhand V, Mittal G, Rhee KY, Park SJ, Hui D. A brief review on basalt fibre reinforced polymer composites. Compos B Eng 2015;73: 166–80.

[3]Saravanan D. Rock-rolling - basalt fibres. J Inst Eng 2006;86: 39–45.

[4]Deák T, Czigány T. Chemical composition and mechanical properties of basalt and glass fibres
features: comparison. Textil Res J 2009;79(7):645–51.

[5] Sheldon GL. Formation of fibres from basalt rock. Platin Met Rev 1977;21(1):18–24.

[6] Gutnikov SI, Malakho AP, Lazoryak BI, Loginov VS. A continuous basalt of alumina oxide
effect on fibre properties. Russ J Inorg Chem 2009;54(2):191-6.

[7]Manylov MS, Gutnikov SI, Lipatov YV, Malakho AP, Lazorya BI. Effect of deferrization on continuous basalt fibre properties. Mendeleev Commun 2015;25(5):386–8.

[8]Manylov MS, Gutnikov SI, Pokholok KV, Lazoryak BI, Lipatov YV. Crystallization mechanism of basalt glass fibres in air. Mendeleev Commun 2013;23(6):361-3.

[9]Sørensen P, Pind M, Yue Y, Rawlings R, Boccaccini A, Nielsen E. Effect of iron redox state and concentration on the crystallization behavior of iron-rich aluminosilicate glasses. J Non-Cryst Solids 2005;351(14-15):1246-53.

[10] Moiseev EA, Gutnikov SI, Malakho AP, Lazoryak BI. Effect of iron oxides on production and properties of continuous glass fibres. Inorg Mater 2008;44(9):1026–30.
[11] Tatarintseva O, Khodakova N, Uglova T. Dependence of the viscosity of basalt solutions on the chemical composition of the original mineral material. Glass Ceramics 2012;68(10):323–6.
[12] Ivanitsky SG, Gorbachev GF. Continuous basalt fibres: manufacturing aspects and simulation of forming processes. I. The highest level of continuous basalt fibre technologies. Powder Metal Met Ceram 2011;50(3–4):125–9.
[13] Tatarintseva O, Khodakova N. Influence of conditions of production of basalt glasses on their physico-chemical properties and drawing the temperature range of continuous fibres. Glass Phys Chem 2012;38(1):89–95.
[14]Ivanitskii S, Gorbachev G. Continuous basalt fibres: manufacturing aspects and simulation of forming processes. II. Optimization of fibre production technology by simulation of heat exchange processes in fibre nozzles. Powder Metal MetCeram 2011;50(5–6):249–55.
[15]Koroteeva LI, Yaskin AP, Glushenkov VI. Spinning glass and basalt fibres. Fibre Chem 2004;36(2):112–5.
[16]IUPAC . Determining and presenting uncertainties of numerical results of thermodynamic measurements. Pure Appl Chem 1981;53(9):1805–25.
[17]Weibull W. A statistical distribution function of general applicability. J Appl Mech 1951;18:293 -7.
[18]Scheffler C, Förster T, Mäder E, Heinrich G, Hempel S, Mechtcherine V. Aging of alkali-resistant glass and basalt fibres in alkaline solutions: assessment of failure stress with a Weibull distribution function. J Non-Cryst Solids 2009;355(52–54):2588–95.
[19]Greco A, Maffezzoli A, Casciaro G, Caretto F. Mechanical properties of basalt fibres and their adhesion to polypropylene matrices. Compos B Eng 2014;67: 233–8 .
[20]Zinck P, Pays MF, Rezakhanlou R, Gerard JF. Extrapolation methods at short gauge lengths based on the weakest link concept for fibres exhibiting multiple failure modes. Philos Mag A 1999;79(9):2103–22.
[21]Bader M, Priest A. Statistical aspects of fibre and bundle strength in hybrid composites. In: Hayashi T, Kawata K, Umekawa S, editors. Prog. Sci. Most. composites. 1982. p. 1129–36. ICCM-IV Tokyo.
[22]Watson A, Smith R. Testing statistical theories for fibrous materials based on experimental data. J Mater Sci 1985; 20(9):3260-70.
[23]Gnädinger F, Middendorf P, Fox B. Effects of carbon fibre sizes and matrix resins on fibre-matrix adhesion: flexural and shear measurements of CFRP-laminates. In: Bonten C, Kreutzbruck M, editors. Proc. 25th interview. Plastic. 2017. p. 145–51. Stuttgart.
[24]Thomason J. Effect of fibre properties on the performance of glass fibre reinforced polyamide 6,6. Compos Sci Technol 1999;59(16):2315–28.
[25]Wei B, Cao H, Song S. Environmental resistance and mechanical performance of basalt and glass fibres. Mater Sci Eng, A 2010;527(18–19):4708–15.
[26] Urinov, K. O., Jumanov, K. A., Khidirov, A. M., Urinov, S. K., Abdiyev, J. M., Jumaboyev, T. A., & Eshmirzayev, M. R. (2020, April). Magnetocaloric effect in polycrystalline cobalt. In *Journal of Physics: Conference Series* (Vol. 1515, No. 2, p. 022079). IOP Publishing.
[27] Saidov, A. S., Saparov, D. V., Usmonov, S. N., Kutlimratov, A., Abdiev, J. M., Kalanov, M., ... & Akhmedov, A. M. (2021). Investigation of the Crystallographic Perfection and Photoluminescence Spectrum of the Epitaxial Films of (Si2) 1-x (GaP) x

\left(0≤x≤1\right) Solid Solution, Grown on Si and GaP Substrates with the Crystallographic Orientation (111). *Advances in Condensed Matter Physics*, *2021*, 1-8.
[28] Saidov, A. S., Usmonov, S. N., Karshiev, A. B., & Abdiev, J. M. (2022, December). Influence of the varizonal Si1-xGex solid solution composition on the thermovoltaic effect in n–Si–p–Si (1-x) Gex structure. In *IOP Conference Series: Earth and Environmental Science* (Vol. 1112, No. 1, p. 012040). IOP Publishing.